

# Measurement of Thin Film Integrated Passive Devices on SiC through 500°C

Zachary D. Schwartz<sup>1</sup>, George E. Ponchak<sup>2</sup>, Samuel A. Alterovitz<sup>2</sup>, Alan N. Downey<sup>2</sup>, and Christine T. Chevalier<sup>1</sup>

<sup>1</sup>Analex Corporation at NASA Glenn Research Center,  
21000 Brookpark Rd, Cleveland, Ohio, 44135 USA, 216-433-3615

<sup>2</sup>NASA Glenn Research Center, Cleveland, Ohio, 44135 USA

**Abstract** — Wireless communication in jet engines and high temperature industrial applications requires RF integrated circuits (RFICs) on wide bandgap semiconductors such as silicon carbide (SiC). In this paper, thin-film NiCr resistors, MIM capacitors, and spiral inductors are fabricated on a high purity semi-insulating 4H-SiC substrate. The devices are experimentally characterized through 50 GHz at temperatures up to 500°C and the equivalent circuits are deembedded from the measured data. It is shown that the NiCr resistors are stable within 10% to 300°C while the capacitors have a value stable within 10% through 500°C.

## I. INTRODUCTION

There is a growing need for sensors and communication circuits that operate at temperatures of 500°C and above for aircraft engine development and monitoring. Interest has also been expressed in high-temperature electronics for use in the harsh environments of interplanetary exploration, telemetry during mining operations, and in conjunction with advanced automotive systems [1], [2]. Wide bandgap materials, such as SiC, are the substrates of choice when working at temperatures above 300°C [3].

High temperature RF measurements have been previously performed under a number of different circumstances. The impedance of commercially available discrete capacitors and resistors has been tracked for thousands of hours at 250°C [4]. On-wafer RF measurements have been used to evaluate coplanar waveguide to 540°C [5], [6].

This paper describes, for the first time, the on-wafer RF measurement of thin-film passive devices on SiC at temperatures up to 500°C. Equivalent circuit models have been fit to the measured data to determine the effects of high temperature on the circuit elements.

## II. CIRCUIT AND SUBSTRATE DESCRIPTION

One quarter of a high purity semi-insulating (HPSI) 4H-SiC wafer, with a thickness of 409  $\mu\text{m}$  and a room temperature resistivity of greater than  $10^8 \Omega\text{-cm}$ , is used [7]. Before processing, an RCA clean is performed. No insulator is purposely grown on the SiC before or after processing. After processing, a full cleaning process is performed to assure all photoresist and adhesion-promoting material is removed. The coplanar waveguide (CPW) feed lines consist of 20 nm of titanium and 1.5  $\mu\text{m}$

of gold. A full set of TRL calibration standards are fabricated on the wafer, including CPW lines of length 5000, 6700, 8500, and 12500  $\mu\text{m}$  and a 2500  $\mu\text{m}$  reflective short. Three categories of passive devices are fabricated: NiCr thin-film resistors, planar spiral inductors, and metal-insulator-metal (MIM) capacitors. The inductors and capacitors are designed for one-port measurements, while the thin film resistors are measured in both a one-port and two-port configuration.

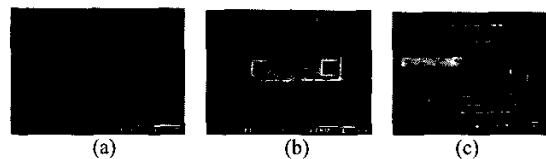


Fig. 1. Scanning electron microscope photographs of (a) thin-film NiCr resistor, (b) MIM capacitor, and (c) 2½-turn spiral inductor.

### A. Resistors

Six different resistors with lengths of 30, 57, 115, 172, 230, and 344  $\mu\text{m}$ , a width of 50  $\mu\text{m}$ , and a NiCr thickness of 70 nm are fabricated on the SiC wafer. Two sets of resistors were fabricated. The first were unpassivated while the second were passivated with a 200 nm layer of silicon nitride ( $\text{Si}_3\text{N}_4$ ) to help prevent the films from oxidizing at high temperatures. A photograph of a NiCr resistor is shown in Fig. 1a.

### B. Capacitors

The metal-insulator-metal (MIM) capacitors are designed with a 750 nm thick bottom gold layer, a 200 nm  $\text{Si}_3\text{N}_4$  dielectric layer, and a 750 nm thick gold upper layer. A plated gold air-bridge connects the top plate of the capacitor to the center conductor of the CPW transmission line. Capacitors of with areas of 3720, 11236, and 18769  $\mu\text{m}^2$  were fabricated. A photograph of a MIM capacitor is shown in Fig. 1b.

### C. Inductors

The planar inductors range in size from ½ turn to 3½ turns. The gold lines are 10  $\mu\text{m}$  wide with a spacing of 10  $\mu\text{m}$  between each turn of the inductor. A gold air-bridge makes the connection from the center turn of the inductor to the transmission line. A photograph of a 2½-turn spiral inductor is shown in Fig. 1c.

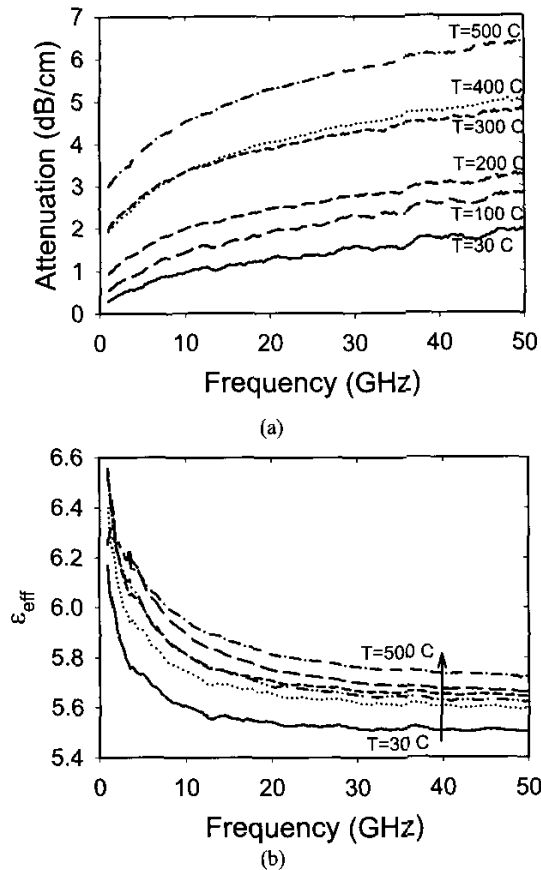


Fig. 2. Measured attenuation (a) and effective permittivity (b) of CPW lines on SiC as a function of frequency and temperature.

### III. MEASUREMENT PROCEDURE

A specially designed RF probe station, previously reported in [8], is used to make measurements from 1 to 50 GHz over the temperature range of 30 to 500°C. The HP8510C network analyzer is first calibrated at room temperature using the CPW standards described above with the multiline thru-reflect-line (TRL) method [9]. After calibration is complete, each passive device is measured and  $S$ -parameter data is recorded. The temperature is then raised, the system is recalibrated at the new temperature, and the devices are measured again. In this way, calibrated measurements are taken at temperatures of 30, 100, 200, 300, 400, and 500°C.

### IV. RESULTS

The attenuation and effective dielectric constant of the CPW is calculated from the results of the multiline calibration. As shown in Fig. 2, the attenuation of the transmission line increases by more than 200% as the temperature is increased to 500°C, while the effective dielectric constant increases by only 5%.

For the passive components, each measured  $S$ -parameter file is fit to an appropriate, physics based

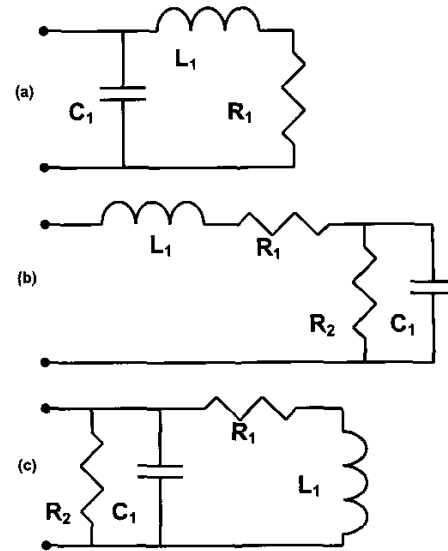


Fig. 3. Equivalent circuit models for (a) thin-film resistor, (b) MIM capacitor, and (c) spiral inductor.

equivalent circuit model to extract the changes in the device characteristics as a function of temperature.

#### A. Resistors

The equivalent circuit model for the thin-film resistor consists of the resistance of the NiCr film ( $R_1$ ), a series inductance ( $L_1$ ), and capacitive coupling between the resistor and the ground lines ( $C_1$ ), as shown in Fig. 3a. It was determined that the leakage through the substrate was very small and is not included in the equivalent circuit model. The resistance of the NiCr films, deembedded from the measured  $S$ -parameter data, increases linearly with length, indicating that the measurements and model deembedding are valid. The NiCr resistance is plotted as a function of length in Fig. 4. At room temperature, the slope is 435  $\Omega/\text{mm}$ , corresponding to a sheet resistance of 21.8  $\Omega/\text{square}$ . The resistance increases as the temperature rises to 200°C, then falls as the temperature continues to 400°C. Below 400°C, the resistance stays within  $\pm 10\%$  of the room temperature value. Above 400°C, however, the resistance value increases dramatically, indicating the resistors have failed. A plot of resistance as a function of temperature for the six devices is shown in Fig. 5. These devices agree with published data on the temperature change of NiCr resistance as a function of temperature through 300°C [10]. A final set of measurements taken at room temperature after the heating cycle confirm that the resistor values are typically 100% higher than their original room temperature values, indicating that the resistor has failed. The unpassivated NiCr resistors had similar characteristics, which shows that the resistor failure is not due to the  $\text{Si}_3\text{N}_4$ .

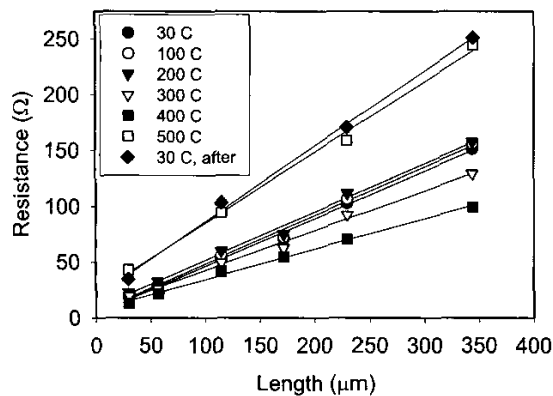


Fig. 4. Measured resistance of passivated resistors as a function of resistor length and temperature.

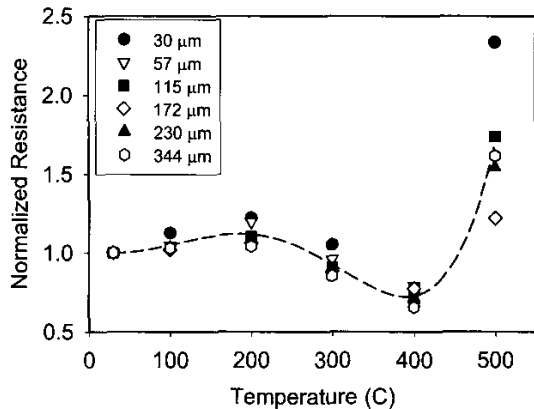


Fig. 5. Measured change in passivated NiCr resistor value from room temperature to 500°C for six resistor lengths. Resistor values are normalized to 1.0.

### B. Capacitors

The equivalent circuit model for the MIM capacitor, shown in Fig. 3b, includes the device's capacitance ( $C_1$ ), conduction through the  $\text{Si}_3\text{N}_4$  dielectric layer ( $R_2$ ), and the series resistance ( $R_1$ ) and inductance ( $L_1$ ) associated with the air-bridge to the top plate of the capacitor. Again, the leakage through the substrate is many orders of magnitude smaller than any leakage through the dielectric, so the substrate effects are ignored.

The deembedded room temperature capacitances of the three capacitor structures are 1.4, 4.2, and 6.5 pF, respectively, indicating a capacitive density of about 0.37 fF/ $\mu\text{m}^2$ . The equivalent capacitance values of six various devices—two of each size, normalized to 1.0—are shown in Fig. 6. At every temperature up to 500°C, the devices are within 10% of the room temperature value. After returning the devices to room temperature, their capacitance values were 1 to 5% higher than the original values. Ellipsometry measurements verify that the  $\text{Si}_3\text{N}_4$  thickness and density did not change during the heating process. The increase in capacitance is most probably due to a decrease in the capacitors' air-bridge heights.

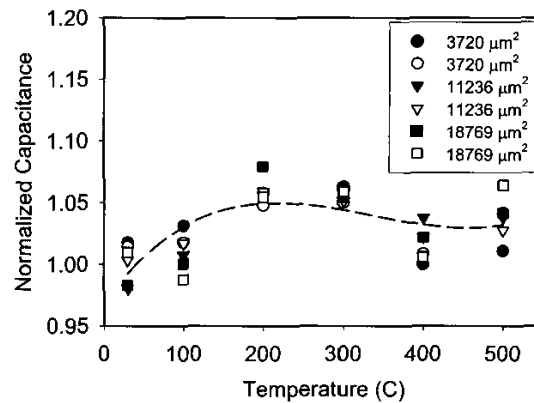


Fig. 6. Measured change in capacitor value from room temperature to 500°C for six capacitors. Capacitor values are normalized to 1.0

### C. Inductors

The equivalent circuit for the spiral inductor, shown in Fig. 3c, includes the device's series inductance ( $L_1$ ) and resistance ( $R_1$ ) as well as capacitive coupling between inductor turns ( $C_1$ ). Leakage through the substrate is included in the inductor model as  $R_2$ . At room temperature, the inductors have measured inductances of 0.31 nH ( $\frac{1}{2}$  turn), 0.57 nH ( $1\frac{1}{2}$  turn), and 2.03 nH ( $3\frac{1}{2}$  turn), as shown in Fig. 7. The values for all three devices appear constant through 200°C. At 300°C, it is clear that the air-bridges have collapsed and effectively shorted out the additional turns of the larger inductors. The authors have noted that some air-bridges on other wafers have also collapsed at elevated temperatures, but if the plated gold thickness is increased, the air-bridges will survive.

The measured series resistance of the inductor increases linearly with temperature as the gold resistivity increases. The effect of this increasing resistance is a decrease in the quality factor of the inductor. The peak Q values for the  $1\frac{1}{2}$  turn inductor is 7.0 at 30°C, 4.1 at 100°C, and 2.9 at 200°C. The quality factor for this inductor is plotted in Fig. 8.

## VII. CONCLUSION

Thin-film, integrated passive devices on SiC substrates show potential for use in high-temperature, high-frequency integrated circuits. In this work, MIM capacitors are shown to have a stable value within 10% through 500°C and thin-film NiCr resistors are stable within 30% to 400°C. The authors also believe that spiral inductors will be usable through 500°C when the air-bridges are adequately protected and strengthened.

### ACKNOWLEDGEMENT

This work is supported by the NASA's Ultra Efficient Engine Technology program. The authors would like to thank Elizabeth McQuaid for fabricating the devices for test.

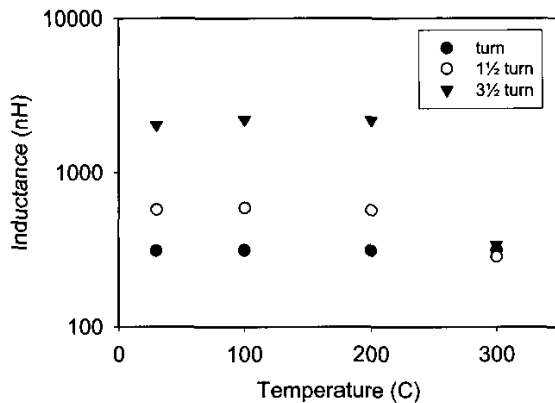


Fig. 7. Measured inductance for three different inductors, room temperature to 300°C. The air-bridges clearly collapse after the 200°C measurement

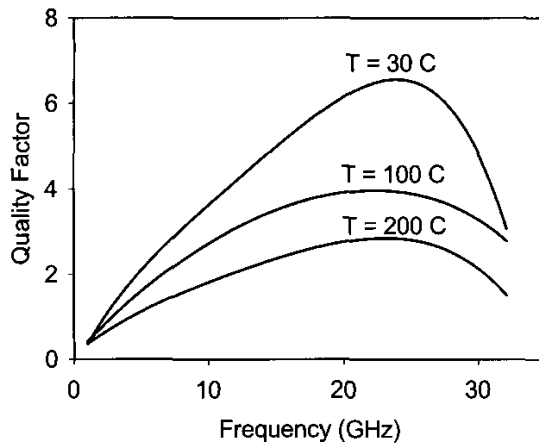


Fig. 8. Measured quality factor for 1½-turn spiral inductor at 30, 100, and 200°C.

- [6] G. E. Ponchak, S. A. Alterovitz, A. N. Downey, J. C. Freeman, and Z. D. Schwartz, "Measured propagation characteristics of coplanar waveguide on semi-insulating 4H-SiC through 800 K," *IEEE Microwave and Wireless Components Letters*, Vol. 13, No. 11, pp. 463-465, (2003)
- [7] Cree wafer number BV0302-11, part number W4TRD8R-0D00.
- [8] Z. D. Schwartz, A. N. Downey, S. A. Alterovitz, and G. E. Ponchak, "High-temperature probe station for use in microwave device characterization through 500°C," 61st ARFTG Conference Digest, pp. 27-35 (2003)
- [9] R. B. Marks, "A multiline method of network analyzer calibration," *IEEE Trans. Microwave Theory and Techniques*, Vol. 39, pp. 1205-1215, (1991)
- [10] D. G. Fink and H. W. Beaty, *Standard Handbook for Electrical Engineers, Eleventh Edition*, McGraw Hill, 1977, p. 4-82.

#### REFERENCES

- [1] C. Johnston, A Crossley, and R. Sharp, "The possibilities for high temperature electronics in combustion monitoring," *Advanced Sensors and Instrumentation Systems for Combustion Processes*, pp. 9/1-9/3 (2000)
- [2] S. Lande, "Supply and demand for high temperature electronics," *The Third European Conference on High Temperature Electronics (HITEN)*, pp. 133-135 (1999)
- [3] P. G. Neudeck, R. S. Okojie, and L.-Y. Chen, "High-Temperature Electronics—A Role for Wide Bandgap Semiconductors?" *Proc. of the IEEE*, Vol 90, No. 6, pp. 1065-1076 (2002)
- [4] R. R. Grzybowski, "High temperature passive components for commercial and military applications," *Energy Conversion Engineering Conference (IECEC)*, Vol 1, pp. 699-704 (1999)
- [5] G. E. Ponchak, Z. D. Schwartz, S. A. Alterovitz, A. N. Downey, and J. C. Freeman, "Temperature dependence of attenuation of coplanar waveguide on semi-insulating 4H-SiC through 540°C," *Electronics Letters*, Vol. 39, Iss. 6, pp. 535-536 (2003)